Ablouh et al. Sustainable Environment Research (2019) 29:5
https://doi.org/10.1186/s42834-019-0004-9

Sustainable Environment Research

RESEARCH Open Access

Chitosan microspheres/sodium alginate hybrid beads: an efficient green adsorbent for heavy metals removal from aqueous solutions

El-houssaine Ablouh[1,2*], Zouhair Hanani[1], Nadia Eladlani[2], Mohammed Rhazi[2] and Moha Taourirte[1]

Abstract

Heavy metal toxicity has demonstrated to be a crucial issue for environment and human health. There has been an increasing ecological and global public health concern related with environmental contamination by these metals. For these reasons, a considerable attention has been paid to design efficient materials for heavy metal removal. This article offers a solution to develop a green adsorbent based on Chitosan Microspheres/Sodium Alginate hybrid beads (CSM/SA) for metal ion elimination from aqueous solutions. The efficiency of this eco-friendly material was divulged using kinetic study for Cr(VI) and Pb(II) removal. Properties of the obtained hybrid beads were improved by correlation between original chitosan microspheres and sodium alginate. Moreover, at different metal concentration, pH solution and contact time, the beads were evaluated in discharged batch operations from Pb(II) and Cr(VI). The maximum adsorption capacity was 180 mg g^{-1} for Pb(II) and 16 mg g^{-1} for Cr(VI). The adsorption kinetics were evaluated using pseudo-first and pseudo-second rate models. Adsorption isotherms were simulated by Langmuir and Freundlich models. This study indicates that the CSM/SA hybrid beads could be developed into a very sustainable technology for highly effective elimination of metal ions from wastewater.

Keywords: Chitosan microspheres, Sodium alginate, Green adsorbent, Heavy metals, Toxicity

Introduction

Contamination of water with toxic compounds, such as heavy metals and dyes, even at low concentration, remains a serious environmental issue due to their dangerous effects on human health [1, 2]. The use of heavy metals arises in various industries such as metallurgy, chemical industry, papermaking, electroplating, steel fabrication, anodizing baths, leather tanning, cement preservation, canning industries and textile [3, 4]. These highly toxic metal ions including lead and chromium exert enormous effects on environment [5, 6]. To overcome this serious problem, considerable attention has been paid to develop new approaches to remove toxic metal ions from polluted environmental matrices, e.g., physicochemical techniques namely precipitation, ion-exchange, electrochemistry, membrane ultrafiltration and chemical adsorption [7]. Among them, adsorption process is more preferable because of its ease and the use of small amounts of chemical additives as well as the possibility of reusing adsorbent materials. Selectivity is the effective property for heavy metal removal alongside to their low-cost. For these reasons, several attempts have been made to develop efficient and economic eco-friendly materials originated from natural sources, which are called “green adsorbents” [8].

Natural polymers are frequently used as adsorbents owing to their reproducibility, biodegradability, biocompatibility, renewability and very low production cost compared to synthetic polymers [9]. In particular, chitosan has been demonstrated to be an appropriate natural compound for metallic ion adsorption [10]. Beside the abundance of this natural biopolymer, chitosan has many functional groups, which enable its binding to various metallic ions through electrostatic attraction or hydrogen bonding [11]. Meanwhile, sodium alginate is a

* Correspondence: lhoussainiblah@gmail.com
[1]Department of Chemistry, Cadi Ayyad University, 40000 Marrakesh, Morocco
[2]Higher Normal School, Cadi Ayyad University, 40000 Marrakesh, Morocco

binary heteropolymer, containing alternating blocks of linearly organized 1–4 linked α-L-guluronic and β-D-mannuronic acid [12]. The presence of carboxylic and hydroxyl groups in alginate can bind metallic ions [13]. However, sodium alginate is soluble in water, which generates a difficult separation from aqueous solution. To overcome the solubility drawback of sodium alginate, sodium was substituted by calcium [14].

The conception of chitosan microspheres and their dispersion in alginate matrix to produce millimeter-sized hybrid beads is a viable alternative adsorbent. The new functional groups are combined to increase the adsorption sites and metal adsorption selectivity. Many studies have concentrated on the use of hybrid beads by mixing two or more components with different physical or chemical properties for the removal of heavy metals [15]. The stabilization of bead-based polymers was carried out via cross-linking or grafting processes [16].

The aim of this study is to shed light into an effective strategy to eliminate heavy metal ions like Pb(II) and Cr(VI) using a novel eco-friendly adsorbent based on chitosan microspheres (CSM) and sodium alginate (SA) and calcium as a cross linking agent. After physico-chemical characterizations of this green adsorbent (CSM/SA), an intensive work was made to evaluate its efficiency through Pb(II) and Cr(VI) ion removal from aqueous system. Then, the effects of contact time, pH, temperature and initial concentration of metal ions on the adsorption capacity of CSM/SA hybrid beads were studied. Finally, kinetics equilibrium and isotherms studies were carried out to explain the adsorption process of Pb(II) and Cr(VI) by CSM/SA hybrid beads.

Materials and methods

Materials

Sodium alginate with average molecular weight 250–360 kDa and viscosity 5–40 cP was purchased from Sigma-Aldrich. Chitosan was prepared according to our previous study [17]. Lead chloride powder (98%), 37% hydrochloric acid, sodium hydroxide, acetic acid and calcium chloride dehydrate were purchased from Analar Normapur. Cr(VI) stock solution was prepared from potassium salts of dichromate ($K_2Cr_2O_7$). All reagents were of analytical grade and were used as received without further purification.

Preparation of CSM

The CSM was prepared according to the procedure used by Berthold and his coworkers [18], with some modifications. Briefly, chitosan solution was obtained by dissolving chitosan in 1 vol% acetic acid solution. Then, sodium sulfate solution 25 wt% was slowly added (4 mL h^{-1}) to chitosan solution at 300 rpm. Finally, after 3 h of magnetic stirring, chitosan microspheres were collected by centrifugation at 4000 rpm for 20 min, and washed with deionized water.

Preparation of CSM/SA hybrid beads

The CSM/SA hybrid beads were prepared by mixing chitosan microspheres and sodium alginate solution. To begin with, 1 g of sodium alginate was dissolved in 100 mL of deionized water with a constant stirring. Then, the previous dispersion of chitosan microspheres was dropped into a homogeneous alginate solution under magnetic stirring (400 rpm) for 4 h at room temperature. By mixing above prepared solutions, an emulsion was formed. The obtained emulsion was added drop wise to 0.2 M calcium chloride solution, under continuous magnetic stirring to complete the cross-linking process. The formed CSM/SA beads were washed three times with deionized water and then dried.

Characterization of CSM/SA beads

The functional groups of CSM/SA hybrid beads were analyzed using Fourier Transform Infrared Spectroscopy (FTIR, Jasco-6030) operated at 4 cm^{-1} over a range of 4000–400 cm^{-1} by attenuated total reflection (ATR). Surface morphology of CSM/SA hybrid beads was obtained using Scanning Electron Microscopy (SEM, Tescan, Vega3), with an accelerating voltage of 20 kV. Energy dispersive X-ray (EDX) analyzer was employed to divulgate the different elements presenting in CSM/SA before and after adsorption. The thermal properties of CSM/SA beads were also studied using thermogravimetry (TGA)-differential thermal analysis (DTA) (Labsys Evo TGA/STA-EGA) and differential scanning calorimetry (DSC, Perkin Elmer). Both analytical techniques were carried out with a heating rate of 10 °C min^{-1}, under nitrogen flow. The pH drift method was used for the determination of the point of zero charge (PZC) of CSM/SA beads [15]. 50 mL of NaCl (0.01 M) solution was taken in a series of fives Erlenmeyer flasks. The range of initial pH values was adjusted between 2 and 10 by adding 0.1 M NaOH and 0.1 M HCl. Then, 0.01 g of correctly weighed CSM/SA beads was added to each flask shaking at 300 rpm for 24 h then the final pH was noted. BET surface area of CSM/SA adsorbent was measured using surface area analyzer (Micrometritics, ASAP 2010) at 77 K.

Batch experiments of heavy metals ion adsorption

Adsorption of Cr(VI) and Pb(II) was carried out using the bottle point methods. Metallic ion solutions were prepared by dissolving $PbCl_2$ and $K_2Cr_2O_7$ in distilled water. 0.1 M of NaOH and HCl was used to regulate the solution pH. The concentrations of metal solutions were measured using an atomic absorption spectrophotometer at 217 and 370 nm for Pb(II) and Cr(VI),

respectively. The effect of pH solution on adsorption process was studied in the pH range of 2–10 for Cr(VI) and 2–6 for Pb(II). The effects of solution temperature (20–55 °C), adsorbent dose (5–35 mg), contact time (0–260 min) and metallic ion concentration (25–300 mg L^{-1}) on removal efficiency were investigated in a batch system.

The adsorption capacity of metallic ions, q_e (mg g^{-1}), was calculated according to the following Eq. (1).

$$q_e = \frac{(C_i - C_e)}{W} \times V \quad (1)$$

The removal efficiency (%) of metallic ions can be expressed using the Eq. (2).

$$\%adsorption = \frac{(C_i - C_e)}{C_i} \times 100 \quad (2)$$

The adsorption capacity of metallic ions q_t (mg g^{-1}) at time "t" can be obtained by Eq. (3).

$$q_t = \frac{(C_i - C_t)}{W} \times V \quad (3)$$

Where C_i, C_e and C_t are respectively the initial, equilibrium and any time of metallic concentration (mg L^{-1}). V is the volume of metallic solution (L) and W is the mass of CSM/SA (g).

Results and discussion

Characterization studies

The TGA-DTA analysis of CSM/SA adsorbent are illustrated in Fig. 1a. It displays four stages thermal degradation of the hybrid beads. The first step was from 25 to 240 °C (weight loss 9.7%) corresponding to the entrapped water molecules in the network [19]. The second and third weight losses observed between 240 and 370 °C is due to biopolymers decomposition. The last stage of the thermal degradation of CSM/SA beads between 370 and 525 °C was attributed to the formation of Na_2CO_3 with a weight loss of 17.1% [20–22]. It is worth noting that the DTA features are consistent with the TGA results. The first DTA peak (endothermic) indicates the energy required to evaporate water physically adsorbed in CSM/SA beads. The two exothermic peaks at 248 and 347 °C were attributed to the energy released from burning organic products. However, the exothermic peak at 447 °C corresponds to the formation of Na_2CO_3.

The DSC curve of CSM/SA beads was recorded from 0 to 400 °C (Fig. 1b). An endothermic peak at 64 °C, corresponds to water evaporation, this is consistent with the results obtained by TGA. Three exothermic peaks can be observed, at 277, 349 and 373 °C due to thermal degradation of organic materials of the adsorbent.

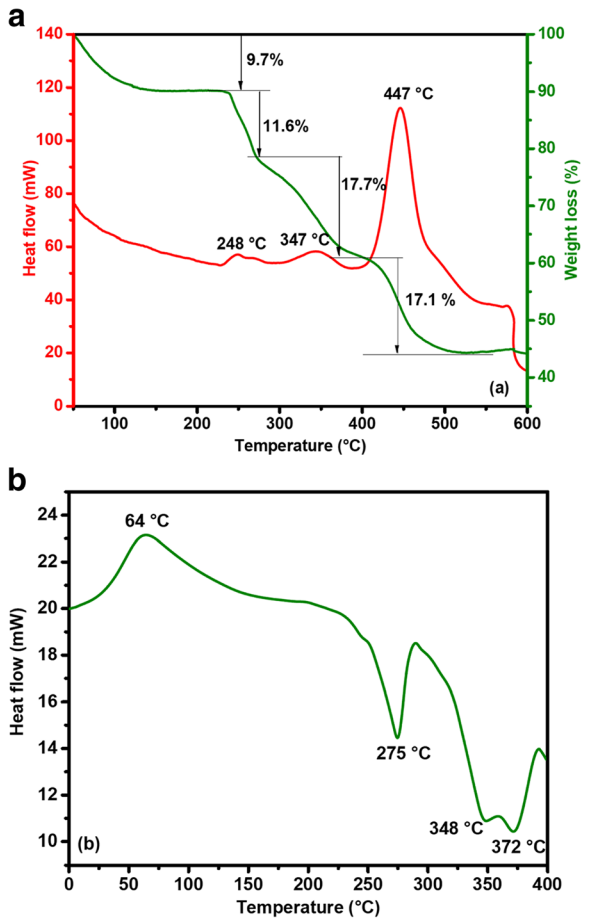

Fig. 1 Thermal behavior of CSM/SA hybrid beads: **a** DTA/TGA thermograms and **b** DSC curve

Figure 2 shows ATR-FTIR results of CSM/SA hybrid beads before and after adsorption process. The band around 1620 cm^{-1}, attributed to amide I vibration of chitosan microspheres cannot be observed [23]. This can be explained by the overlapping with stronger asymmetric vibration band of COO^- belonging to alginate [7]. The broad peak observed at 3250 cm^{-1} was correspond to the intermolecular hydrogen bonded O-H stretching and stretching vibration N-H [24]. The peaks obtained at 1312, 1019 and 1012 cm^{-1} indicate the presence of OH in-plane bending, C-O stretching and C-O-C bending, respectively [25]. The absence of the peak corresponding to the amine group (1160 cm^{-1}) in the CSM/SA bead spectrum confirms the formation of electrostatic interactions between positively charged amino groups ($-NH_3^+$) of chitosan and negatively charged carboxylic units ($-COO^-$) of alginate [26]. As illustrated in Fig. 2, after Cr(VI) adsorption, it was observed that the stretching vibration peak of -OH or NH_2 at around 3250 cm^{-1} shifted to 3245 cm^{-1}. This indicates the formation of hydrogen bonds between the hydrogen atoms

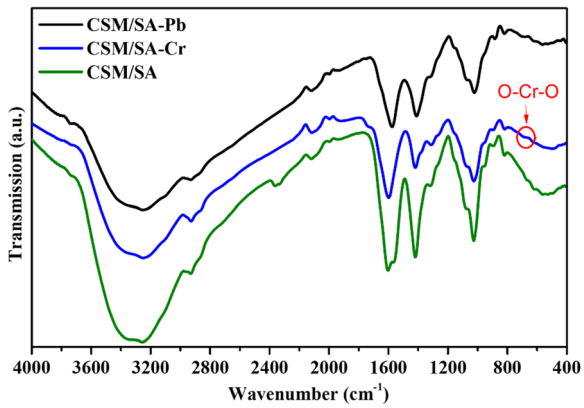

Fig. 2 ATR-FTIR spectra of CSM/SA hybrid beads, (CSM/SA-Pb) CSM/CA hybrid beads loaded Pb(II) and (CSM/SA-Cr) CSM/CA hybrid beads loaded Cr(VI)

on NH_2 groups and O atoms of oxyanion species of Cr(VI) [27]. Meanwhile, the slight shifting characteristic of the peak corresponding to COO bond from 1600 to 1590 cm^{-1} could be indicative of the interactions between COO groups and Cr(VI). These displacements explain the electrostatic interaction between Cr(VI) and OH, COO, NH_3^+ groups. In addition, a new peak appears at 682 cm^{-1} (CSM/SA-Cr) which could be mostly due to O-Cr-O band belonging to Cr species [28].

After adsorption of Pb(II), a shifting of some bands was observed. The stretching vibration of O-H band was significantly shifted from 3250 to 3261 cm^{-1}, and the characteristic peak of the COO bond showed a strong shift from 1600 to 1569 cm^{-1}. These peaks displacement could be due to the coordination effect of the O atom and Pb(II) ions, which indicates the ion exchange between Pb^{2+} and Ca^{2+} on the interlayer surface of CSM/SA [29]. Furthermore, no new obvious absorption band was observed after Pb(II) adsorption.

Using the SEM microscopy, elemental mapping was performed and EDX spectra were collected for CSM/SA sample before and after adsorption of both ions. The results are represented in Figs. 3 and 4. SEM was used to provide an idea on the homogeneity and the microstructure of CSM/SA hybrid beads. Figure 3a exposes that a large number of granular microspheres with a uniform size were dispersed on the surface of alginate. Probably, this may be due to the presence of carboxyl groups of alginate (COO^-) which can interact with amino groups (NH_3^+) of chitosan microspheres [14]. On the other hand, the morphological characteristics of these hybrid beads will be mostly due to the original alginate microstructure, with a slight increase in the specific interfacial area. EDX analysis of hybrid beads confirms the existence of small amount of nitrogen (1.5%) observed on the surface, while the major percentages 38.3, 36.4 and 23.7% correspond to C, Ca and O, respectively (Fig. 4).

The surface area is an important parameter in adsorption study. For this purpose, BET method was applied to evaluate the surface area of CSM/SA adsorbent and found to be 76 $m^2 g^{-1}$. This result indicates that the prepared CSM/SA have a relatively high surface area compared to some adsorbent based chitosan and alginate [30].

In order to have more insights on the chemical composition and the spatial distribution of elements on the surface of CSM/SA adsorbent, the elemental mapping was employed using EDX. The results are outlined in Fig. 4. A homogeneous distribution of the cited elements was approved on CSM/SA hybrid beads before and after metals loaded. Carbon and oxygen corresponding micrographs for the hybrid beads before and after adsorption indicate the distribution of the functional groups on the surface. After adsorption process, Fig. 4c illustrates that the adsorption of lead ions onto CSM/SA induces many changes in the adsorbent surface. Similarly, for chromium ion elimination, SEM micrograph shows glossy and bright microspheres of chitosan on the uniform surface, which indicates a low interaction between Cr(VI) and the adsorbent (Fig. 4b).

From the typical EDX graphs and elemental mapping, a new peak around 2.5 keV appears after adsorption process with dense distribution at CSM/SA surface, was attributed to Pb element (31.6%). Meanwhile, Ca peak disappears in the EDX spectrum after

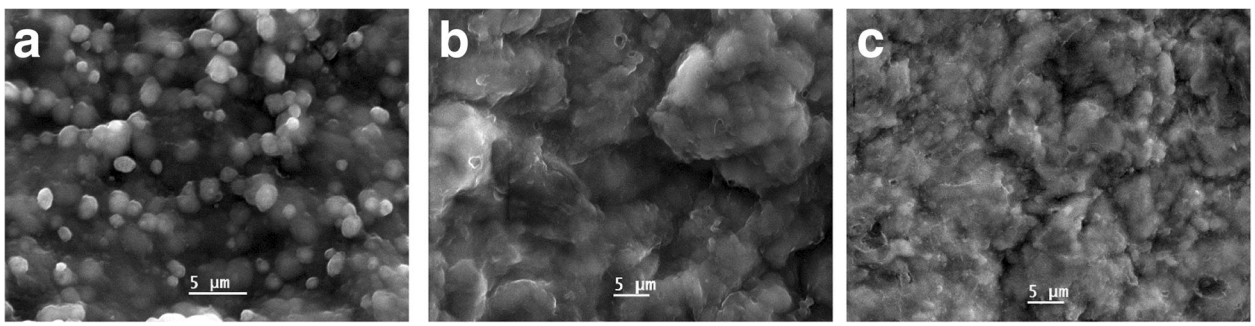

Fig. 3 SEM micrographs of the prepared CSM/SA hybrid beads: **a** before metal adsorption, **b** After Cr(VI) loading, **c** After Pb(II) loading

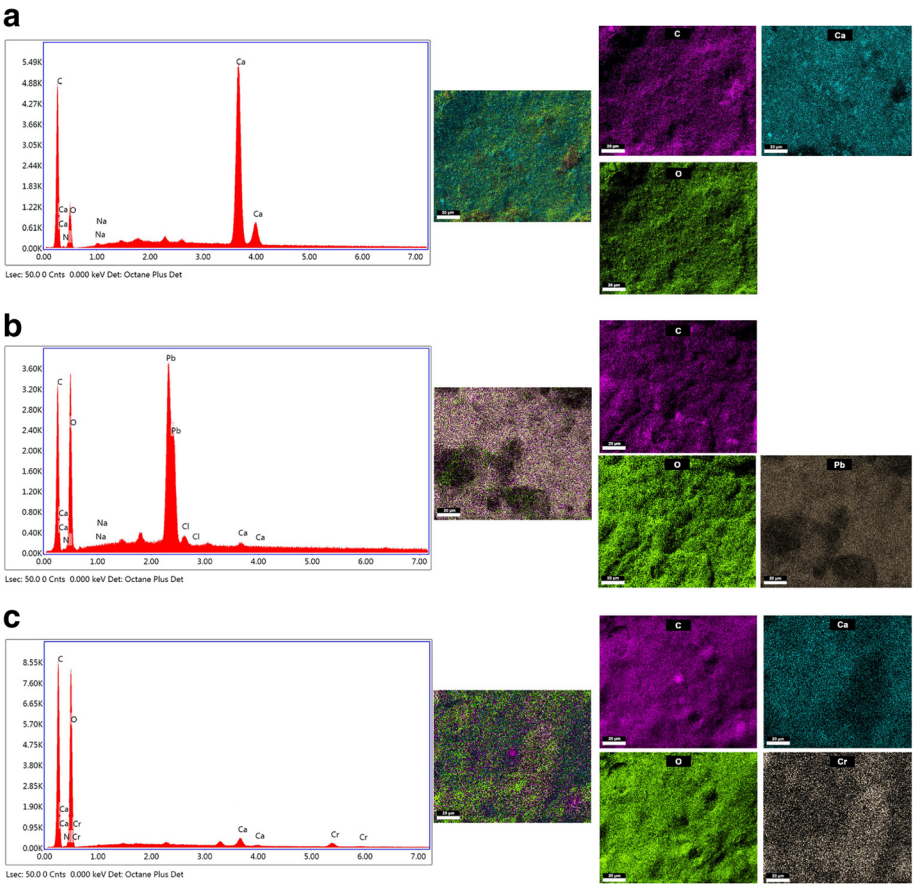

Fig. 4 EDX and elemental mapping of the CSM/SA hybrid beads: **a** before metal adsorption, **b** after Pb(II) loading, **c** after Cr(VI) loading

lead adsorption. In other words, the calcium element was totally removed from CSM/SA adsorbent. This characteristic suggests that the ion exchange might be the main mechanism governing the removal of lead ions from aqueous solutions. The presence of Cl element is probably due to chloride ions from lead chloride solution used in the adsorption process.

In addition, the images of elemental mapping show that chromium (2.3%) is uniformly distributed along the surface of CSM/SA adsorbent. In comparison, the bright contrast spots of Ca (10.5%) were more solidly dispersed at the adsorbent surface as depicted in Fig. 4b. This result suggests that the adsorption mechanism of chromium in the hybrid beads is controlled only by electrostatic attractions [31].

To sum up, based on FTIR, SEM and EDX analyses, the mechanism of Pb(II) removal by CSM/SA hybrid beads was governed by ion exchange between calcium on the adsorbent surface and lead ions in the aqueous solution [12]. Probably, the mechanism for Cr(VI) removal includes mainly electrostatic attractions (Fig. 5).

Factors affecting removal of Pb(II) and Cr(VI) ions

Several parameters affect the adsorption efficiency, such as pH, pH_{pzc}, adsorbent dose, initial metals concentration and temperature.

According to literature, the most important factor influencing the adsorption capacity and removal efficiency of CSM/SA is the initial pH value of the solution. From Fig. 6a, the adsorption of Pb(II) and Cr(VI) was very dependent on pH mainly because it affects the solubility of metal ions and the adsorbent surface charge [14]. Increasing the pH from 3 to 5 resulted a slight enhancement in the adsorption capacity of Pb(II) from 160 to 164 mg g^{-1}, respectively. No precipitation of lead hydroxide or protonation of the carboxyl group occurred in this pH range [12]. However, when the pH value was above 6, the precipitation of insoluble lead hydroxide was observed, inducing a decrease in the removal of Pb(II) ions. Concerning Cr(VI) elimination, the adsorption capacity decreases with increasing pH value, producing a significant reduction in Cr(VI) through basic pH values. As shown in Fig. 6a, when the pH increasing from 3.0 to 7.0, the quantity of Cr(VI) adsorbed onto CSM/SA at equilibrium decreases from 5.0

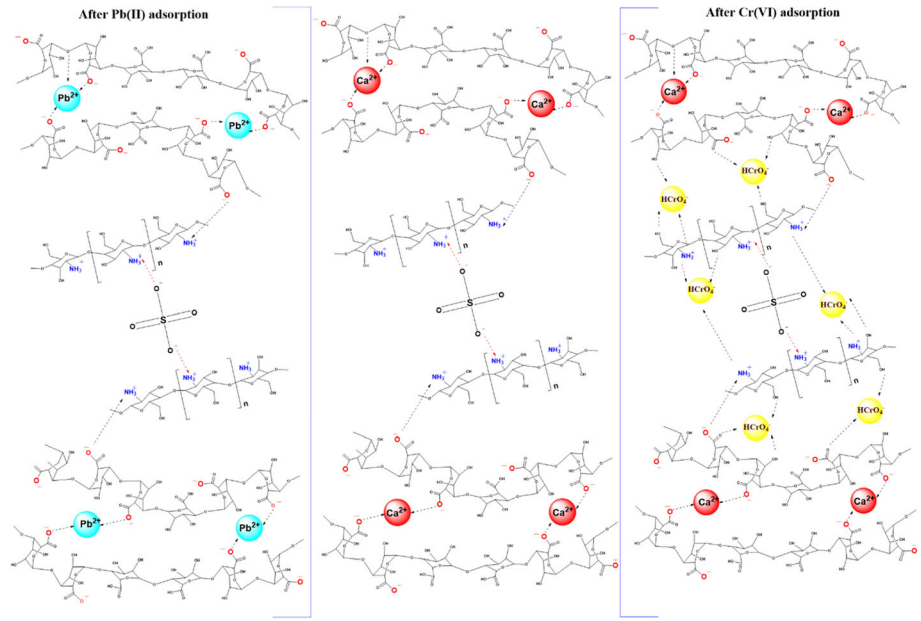

Fig. 5 Proposed mechanism of adsorption of Cr(VI) and Pb(II) ions onto CSM/SA hybrid beads

to 0.5 mg g^{-1}. At different pH levels, it is important to remember that Cr(VI) can occur in various forms: CrO_4^-, $Cr_2O_7^{2-}$ $HCrO_4^-$, and $H_2CrO_4^-$ [32]. When the pH of the medium is between 2 and 4, the predominant specie will be $HCrO_4^-$, and amine groups are easily protonated to produce NH_3^+ species present in CSM/SA surface which increases the electrostatic attraction between the anionic chromium and the protonated amine functionalities. Therefore, the pH of 3.0 and 5.2 could be selected as an optimum pH values for the consequent experiments for Cr(VI) and Pb(II), respectively.

pH_{pzc} is another important parameter, where the PZC of the adsorbent governs the adsorption process. It is the pH value where the net surface charge of the adsorbent corresponds to zero, and it offers the possible mechanism about the electrostatic interaction between adsorbent and adsorbate [33]. At a pH below 6.6 (Fig. 6b), the CSM/SA surface is positively charged. The functional groups such as NH_3^+, H_3O^+, $COOH^+$ were protonated and positively charged, thus preventing metal adsorption due to electrostatic repulsion [5]. There might be another adsorption mode such as cationic exchange with the protonated carboxylic groups in acidic solutions, ionic exchange between calcium ions bound and carboxyl groups by complexation of metal cations on carboxylate, amino and hydroxyls groups present in CSM/SA adsorbent surface [7]. For a pH < 3, most of the carboxylate groups are protonated. In this case, the mechanism in metal binding should be ion-exchange between protons and free metal cations [34]. When the pH value was increased, the deprotonation of carboxylic acid and amino groups allows the ionic exchange between Pb^{2+} and Ca^{2+} ions. This was confirmed by EDX and elemental mapping before and after adsorption (Fig. 4). Similar results was reported by Gopalakannan and Viswanathan [19]. The positively charged surface at pH < 6.6 promotes the retention of anionic contaminants. At an initial pH = 2, Cr(VI) mainly exists in anionic form ($HCrO_4^-$). According to the pH and pH_{pzc} results, the electrostatic attraction between anionic $HCrO_4^-$ and the positively charged surface of the CSM/SA is responsible for Cr(VI) adsorption.

The adsorption time is one of the principal parameters that influences the elimination toxic species from aqueous solution [29]. The influence of contact time on the elimination efficiency of Pb(II) and Cr(VI) ions using CSM/SA hybrid beads is illustrated in Fig. 6c. During first 115 min of the process, it was noticed that the removal efficiencies of Cr(VI) and Pb(II) were 6 and 45%, respectively. By increasing the contact time to 190 min, the pervious adsorbed values of Cr(VI) and Pb(II) increased gradually to 7 and 55%, respectively. After 200 min to the end of shaking time, the values of removal efficiency were nearly constant due to the saturation of active sites and the attainment of dynamic equilibrium stage. The metal ions removed by CSM/SA adsorbent reached the equilibrium after 200 min for Pb(II) and 220 min for Cr(VI). Therefore, 200 and 220 min could be considered as the equilibrium time.

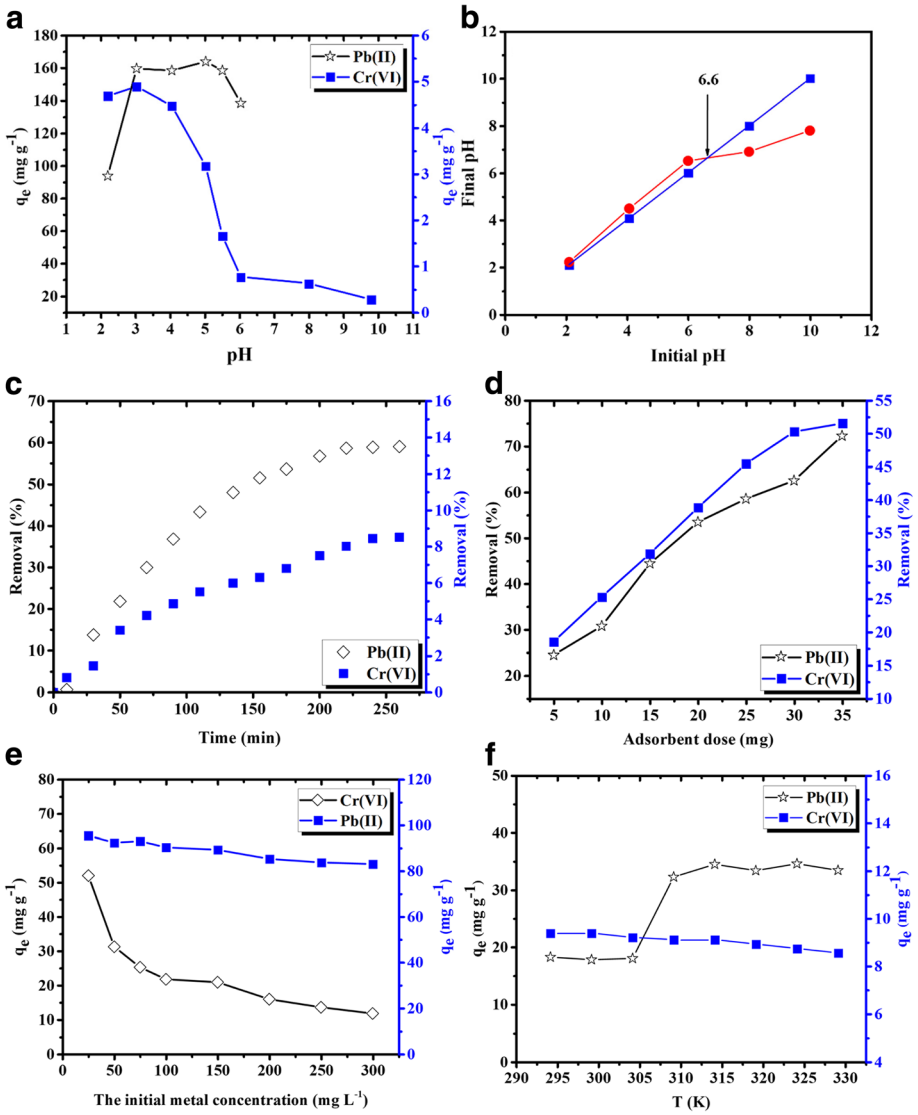

Fig. 6 **a** Effect of the initial pH [initial concentration of Pb(II) and Cr(VI): 100 mg L^{-1}; adsorbent dose: 0.06 g; T = 25 °C; contact time: 135 min], **b** point of zero charge, **c** contact time [initial concentration of Pb(II) and Cr(VI): 100 mg L^{-1}; adsorbent dose: 0.06 g; T = 25 °C; initial pH for Pb(II) and Cr(VI); 3.0 and 5.2], **d** adsorbent dose [initial concentration of Pb(II) and Cr(VI): 100 mg L^{-1}; T = 25 °C; initial pH for Pb(II) and Cr(VI); 3.0 and 5.2; contact time: 250 min], **e** initial metal concentration [T = 25 °C; initial pH for Pb(II) and Cr(VI); 3.0 and 5.2; contact time: 250 min; adsorbent dose: 0.06 g] and **f** temperature [initial concentration of Pb(II) and Cr(VI): 100 mg L^{-1}; adsorbent dose: 0.06 g; contact time: 135 min; adsorbent dose: 0.06 g] for the adsorption of Pb(II) and Cr(VI) onto CSM/SA hybrid beads

The influence of adsorbent dose on the percentage of metal ion removal under optimal conditions was studied. According to Fig. 6d, the amount of adsorbent used during the adsorption influenced the removal percentage. The adsorption of Pb(II) and Cr(VI) ions was attained about 25 and 17% removals when 5 mg of CSM/SA hybrid beads were used. At the highest adsorbent amount (35 mg), the elimination efficiency reaches 72% for Pb(II) and 51% for Cr(VI). These may be attributed to the presence of greater number of adsorbent sites and surface area at higher adsorbent dose.

Initial metal ion concentration plays an imperative role in the adsorption of metal ions. The adsorption was studied using the different initial concentrations of metal ions (25–300 mg L^{-1}), the results shows that the percentage of elimination decreases with increasing the initial metal ion concentration due to the saturation of the adsorption sites on the CSM/SA adsorbent surface as illustrated in Fig. 6e. However, the quantity of metal ions adsorbed per unit weight of adsorbent (mg g^{-1}) was found to increase with increasing initial concentration. The capacity was 40, 156 and 160 mg g^{-1} respectively

for the initial Pb(II) concentration 25, 100 and 300 mg L^{-1}. While for Cr(VI), the adsorption capacities for the initial concentration 25, 100 and 300 mg L^{-1} are 6, 8 and 14 mg g^{-1}, individually. However, with additional increase of the initial metal ion concentration, the adsorption capacities enhanced slowly or even continued unaffected, signifying that the number of active sites on CSM/SA adsorbent could be the factor limiting its adsorption capacities. Therefore, the maximum adsorption value of metal ions on adsorbent was obtained at higher concentration of metal ions due to saturation of available active sites.

Environmental temperature is a significant factor that can influence the efficiency of the adsorbent during the adsorption process [35]. The adsorption capacities were compared at different stabilized temperatures under the same experimental conditions for CSM/SA adsorbent. Figure 6f reveals that the adsorption of Pb(II) was increased after raising the temperature from 30 to 55 °C, resulting in an enhancement of adsorption capacity, which indicates an endothermic process. On the other hand, the chromium removal is independent of temperature.

Data analysis of the adsorption kinetics

The adsorption kinetics data of Pb(II) and Cr(VI) on CSM/SA adsorbent were studied using three different kinetic models: pseudo-first-order, pseudo-second-order and intraparticle diffusion models [33], which are usually expressed, respectively, as follow:

$$log(q_e - q_t) = logq_e - \left(\frac{k_1}{2.303}\right)t \quad (4)$$

$$\frac{1}{q_t} = \frac{1}{k_2 q_e^2} \times \frac{1}{t} + \frac{1}{q_e} \quad (5)$$

$$q_t = k.t^{1/2} + C \quad (6)$$

Where k_2 represents the second-order rate constant (g mg^{-1} min), q_e and q_t are adsorption capacities (mg g^{-1}) corresponding to equilibrium and time t (min), respectively. k_1 is the pseudo-first order rate constant (min^{-1}) and k (mg g^{-1} $min^{-1/2}$) is the intra-particle diffusion constant. The kinetics plots for metal ions absorption onto CSM/SA adsorbent are presented in Fig. 7.

The kinetic parameters and coefficient of determination R^2 for adsorption of metal ions on CSM/SA adsorbent were determined by linear regression analysis (Table 1). It indicates that for Pb(II) the pseudo-first-order model present the best sorption process with a highest coefficient of determination ($R^2 > 0.99$) compared to the pseudo-second-order model ($R^2 < 0.95$). This result designates that the adsorption process of Pb(II) is complicated in rate-determining step. For Cr(VI) adsorption, according to the correlation coefficients ($R^2 > 0.99$), the adsorption process fits well the pseudo-second-order model and the theoretical values (q_e cal) was close to the experimental values (q_e).

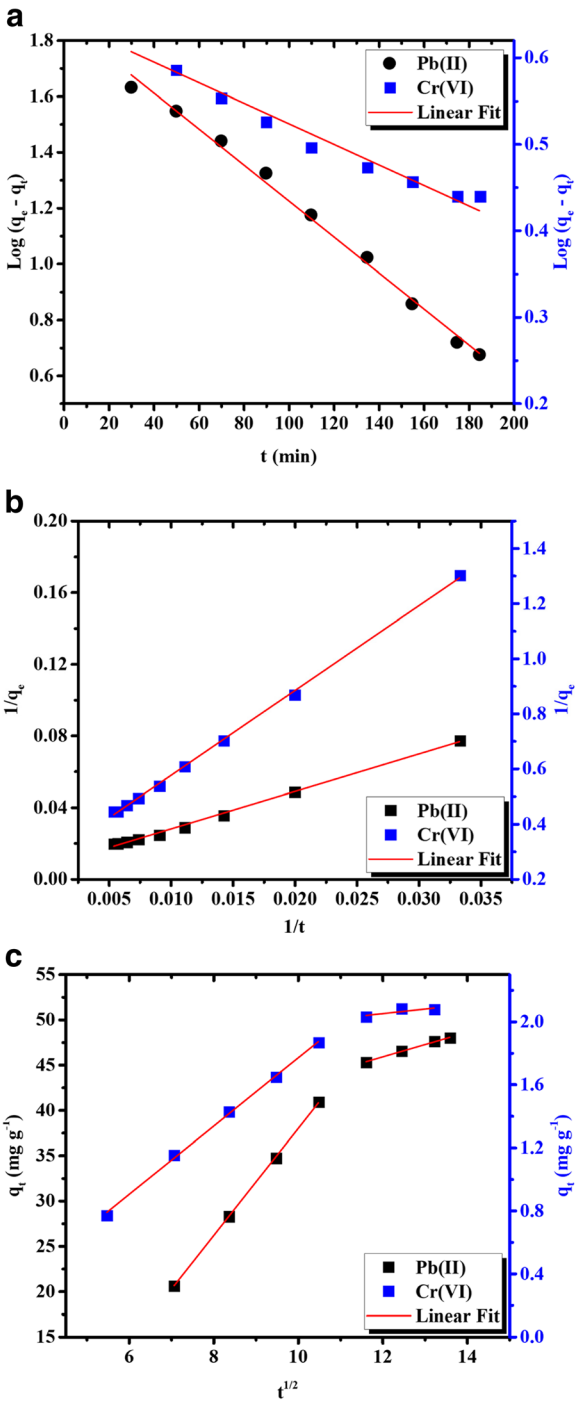

Fig. 7 The pseudo-first-order (**a**), pseudo-second-order (**b**) and intraparticle diffusion (**c**) plot for Pb(II) and Cr(VI) ions adsorption onto CSM/SA hybrid beads

The mechanism of metal ion adsorption was studied by the intra-particle diffusion model by plotting the

Table 1 Kinetic parameters for the adsorption of Pb(II) and Cr(VI) ion onto CSM/SA hybrid beads

		Pseudo-first-order			Pseudo-second-order			Intraparticle Diffusion	
Ion	$q_e$exp (mg g^{-1})	$q_e$cal (mg g^{-1})	k_1 (min^{-1})	R^2	$q_e$cal (mg g^{-1})	k_2 (g mg^{-1} min^{-1})	R^2	k (mg g^{-1} $min^{-1/2}$)	R^2
Pb(II)	51	74	0.014	0.995	86	0.0022	0.949	4.9	0.884
Cr(VI)	2.2	4.4	0.0027	0.967	3.6	0.0025	0.997	0.19	0.989

amount of the adsorbed metal at time t (q_t) and the square root of time ($t^{1/2}$). According to this model, if the plot of q_t versus $t^{1/2}$ gives a straight line, then the adsorption process is governed by intra-particle diffusion, and if the data reveal multi-linear plots, then two or more steps rule the adsorption process [36]. From Fig. 7c, the graph presents two distant linear plots, which indicates that the adsorption process was not governed uniquely by intraparticle diffusion. In the linear part, the adsorption rate of Pb(II) and Cr(VI) ions is high due to the external surface adsorption. The second plateau indicated the slowing of intra-particle pore diffusion.

Adsorption isotherms

To determine the maximum metal adsorption capacities of CSM/SA hybrid beads, Langmuir (Eq. (7)) and Freundlich (Eq. (8)) isotherms models have been used [33]. Both models can be computed by the following equation:

$$\frac{1}{q_e} = \frac{1}{bC_e k_L} + \frac{1}{b} \tag{7}$$

$$\ln q_e = \frac{1}{n} \ln C_e + \ln k_f \tag{8}$$

Where q_e is the amount of metal ions adsorbed per unit weight of the adsorbent (mg g^{-1}). C_e is the equilibrium concentration of metal ions in solution (mg L^{-1}), b (L mg^{-1}) is Langmuir isotherm constant that relates to the energy of adsorption, K_L is the Langmuir equilibrium constant, K_F specifies the adsorption capacity and 1/n is a numerical value associated to the adsorption intensity.

To evaluate the adsorption process according to Langmuir isotherm, a separation factor was calculated as follow (Eq. (9)):

$$R_L = \frac{1}{1 + bC_0} \tag{9}$$

The simulating curves of the Langmuir and Freundlich models are shown in Fig. 8. The fitted constants with regression coefficients (R^2) are summarized in Table 2. It was found that the obtained adsorption data are in accordance to the Langmuir isotherm model with R^2 = 0.992 and 0.979 for Pb(II) and Cr(VI), respectively. The maximum adsorption capacity of CSM/SA hybrid beads were 189 and 16 mg g^{-1} for Pb(II) and Cr(VI), respectively. These values are much higher than those reported by Ren et al. [31] for sodium alginate-carboxymethyl cellulose gel beads (1.7 mg g^{-1}) [34]. The R_L values are in the range of $0 < R_L < 1$, which indicate that the adsorption of chromium and lead by CSM/SA adsorbent was favorable.

It is encouraging to compare our findings with those reported in literature with other adsorbents.

The maximum adsorption capacities of Pb(II) and Cr(VI) on chitosan and alginate adsorbents reported in the literature are listed in Table 3.

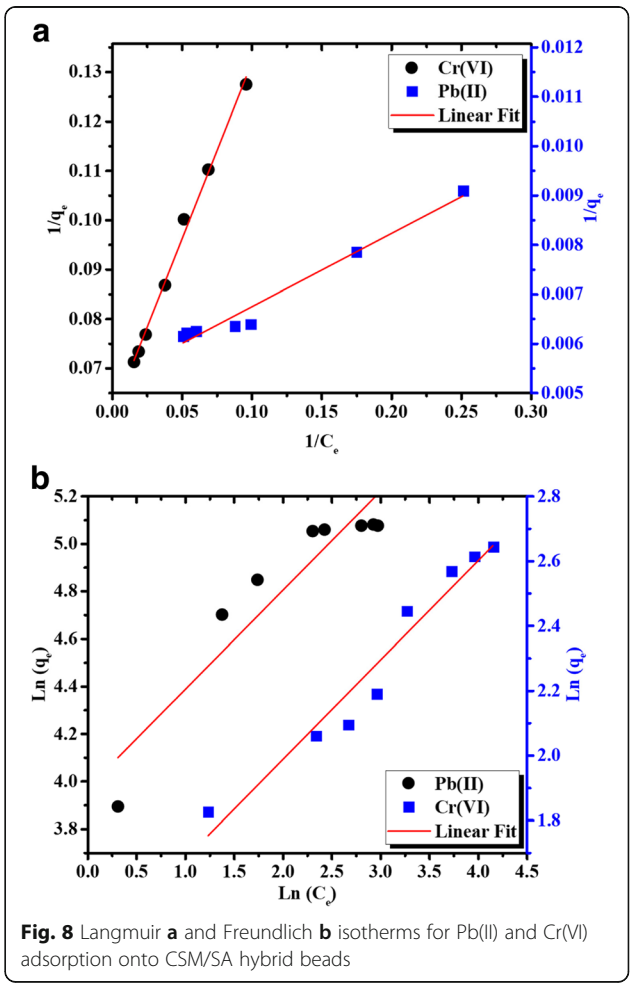

Fig. 8 Langmuir **a** and Freundlich **b** isotherms for Pb(II) and Cr(VI) adsorption onto CSM/SA hybrid beads

Table 2 Various isotherms parameters of Pb(II) and Cr(VI) ions adsorption onto CSM/SA hybrid beads

Ion	q_e exp. (mg g^{-1})	q_{max} (mg g^{-1})	Langmuir			Freundlich		
			K_L (L mg^{-1})	R_L	R^2	K_F ((mg g^{-1}) (L $mg^{-1})^{1/n}$)	N	R^2
Pb(II)	161	189	0.34	0.021	0.992	10.6	2.07	0.915
Cr(VI)	14	16	24	0.0063	0.979	3.9	3.26	0.949

Table 3 Maximum adsorption capacity of different adsorbents based biopolymers used for the removal of Pb(II) and Cr(VI)

Adsorbents	q_{max} (mg g^{-1})		References
	Pb(II)	Cr(VI)	
Chitosan microspheres/sodium alginate hybrid beads	189	16	This study
Chitosan alginate-beads	24	–	[37]
Chitosan-crosslinked-poly(alginic acid) nanohydrogel	–	25	[38]
Sodium alginate-polyanilinenanofibers	–	73	[39]
Chitosan coated calcium alginate beads	107	–	[14]
Graphite doped chitosan composite	6.7	–	[40]
Silica nanopowders/alginate composite	83	–	[41]

Conclusions

The present study was undertaken to evaluate the efficiency of newly developed green adsorbent based on chitosan microspheres/sodium alginate hybrid beads for the elimination of Cr(VI) and Pb(II) in aqueous synthetic solutions. Resultant hybrid beads were characterized by TGA, DSC, FTIR, SEM with EDX elemental mapping and were subjected for metal ion removal in batch process. The most obvious findings to emerge from this study are summing as follows:

1. TGA/DTA and DSC analyses of the prepared CSM/SA beads reveals high thermal stability.
2. FTIR results indicate mutual interaction between chitosan microspheres and sodium alginate.
3. The surface characterizations of the adsorbent confirm the distinct morphology and characteristics of chitosan microspheres dispersed in sodium alginate matrix before and after adsorption.
4. EDX elemental mapping confirms that the quantity of adsorbed Pb^{2+} ions is directly correlated to the amount of Ca^{2+} at the surface of CSM/SA hybrid beads. However, the electrostatic attraction is responsible for chromium retention.
5. CSM/SA green adsorbent shows high adsorption capacity of 188 and 16 mg g^{-1} for Pb(II) and Cr(VI), respectively.
6. Equilibrium data fitted very well to the Langmuir isotherm, confirming the monolayer adsorption capacity of both ions onto CSM/SA hybrid beads.

These findings clearly demonstrate that chitosan microspheres/sodium alginate hybrid beads are expected to be economically viable for large-scale removal of Pb(II) and Cr(VI) ions from aqueous solutions.

Acknowledgments

The authors gratefully acknowledge Center of Analysis and Characterization (CAC) - Cadi Ayyad University (Morocco) for providing instrumental facilities for sample characterizations.

Authors' contributions

The manuscript was mainly based on a draft written by EA, and written through contributions of all authors. All authors read and and approved the final manuscript.

Competing interests

The authors declare that they have no competing interests.

Publisher's Note

Received: 23 June 2018 Accepted: 13 November 2018
Published online: 19 March 2019

References

1. Dutta K, De S. Aromatic conjugated polymers for removal of heavy metal ions from wastewater: a short review. Environ Sci Wat Res. 2017;3:793–805.
2. Abdel-Halim ES, Al-Deyab SS. Removal of heavy metals from their aqueous solutions through adsorption onto natural polymers. Carbohyd Polym. 2011; 84:454–8.
3. Eladlani N, Dahmane E, Ouahrouch A, Rhazi M, Taourirte M. Recovery of chromium(III) from tannery wastewater by nanoparticles and whiskers of chitosan. J Polym Environ. 2018;26:152–7.
4. Kan CC, Ibe AH, Rivera KKP, Arazo RO, de Luna MDG. Hexavalent chromium removal from aqueous solution by adsorbents synthesized from groundwater treatment residuals. Sustain Environ Res. 2017;27:163–71.
5. Liu W, Zhang JS, Jin YJ, Zhao X, Cai ZQ. Adsorption of Pb(II), cd(II) and Zn(II) by extracellular polymeric substances extracted from aerobic granular sludge: efficiency of protein. J Environ Chem Eng. 2015;3:1223–32.
6. Shahabuddi S, Tashakori C, Kamboh MA, Korrani ZS, Saidur R, Nodeh HR, et al. Kinetic and equilibrium adsorption of lead from water using magnetic metformin-substituted SBA-15. Environ Sci Wat Res. 2018;4:549–58.
7. Wang SY, Vincent T, Roux JC, Faur C, Guibal E. Pd(II) and Pt(IV) sorption using alginate and algal-based beads. Chem Eng J. 2017;313:567–79.
8. Kyzas GZ, Kostoglou M. Green adsorbents for wastewaters: a critical review. Materials. 2014;7:333–64.
9. Algothmi WM, Bandaru NM, Yu Y, Shapter JG, Ellis AV. Alginate-graphene oxide hybrid gel beads: an efficient copper adsorbent material. J Colloid Interf Sci. 2013;397:32–8.
10. Ahmad M, Manzoor K, Ikram S. Versatile nature of hetero-chitosan based derivatives as biodegradable adsorbent for heavy metal ions; a review. Int J Biol Macromol. 2017;105:190–203.
11. Sun XT, Li Q, Yang LR, Liu HZ. Chemically modified magnetic chitosan microspheres for Cr(VI) removal from acidic aqueous solution. Particuology. 2016;26:79–86.
12. Wang ZQ, Huang YG, Wang M, Wu GH, Geng TM, Zhao YG, et al. Macroporous calcium alginate aerogel as sorbent for Pb^{2+} removal from water media. J Environ Chem Eng. 2016;4:3185–92.
13. Cataldo S, Gianguzza A, Milea D, Muratore N, Pettignano A. Pb(II) adsorption by a novel activated carbon – alginate composite material. A kinetic and equilibrium study. Int J Biol Macromol. 2016;92:769–78.

14. Mousa NE, Simonescu CM, Patescu RE, Onose C, Tardei C, Culita DC, et al. Pb^{2+} removal from aqueous synthetic solutions by calcium alginate and chitosan coated calcium alginate. React Funct Polym. 2016;109:137–50.
15. Gopalakannan V, Viswanathan N. Development of nano-hydroxyapatite embedded gelatin biocomposite for effective chromium(VI) removal. Ind Eng Chem Res. 2015;54:12561–9.
16. Kong DL, Wang N, Qiao N, Wang Q, Wang Z, Zhou ZY, et al. Facile preparation of ion-imprinted chitosan microspheres enwrapping Fe_3O_4 and graphene oxide by inverse suspension cross-linking for highly selective removal of copper(II). ACS Sustain Chem Eng. 2017;5:7401–9.
17. Tolaimate A, Desbrieres J, Rhazi M, Alagui A, Vincendon M, Vottero P. On the influence of deacetylation process on the physicochemical characteristics of chitosan from squid chitin. Polymer. 2000;41:2463–9.
18. Berthold A, Cremer K, Kreuter J. Preparation and characterization of chitosan microspheres as drug carrier for prednisolone sodium phosphate as model for antiinflammatory drugs. J Control Release. 1996;39:17–25.
19. Gopalakannan V, Viswanathan N. One pot synthesis of metal ion anchored alginate-gelatin binary biocomposite for efficient Cr(VI) removal. Int J Biol Macromol. 2016;83:450–9.
20. Soares JP, Santos JE, Chierice GO, Cavalheiro ETG. Thermal behavior of alginic acid and its sodium salt. Eclet Quim. 2004;29:57–63.
21. Schnepp Z, Wimbush SC, Mann S, Hall SR. Alginate-mediated routes to the selective synthesis of complex metal oxide nanostructures. Crystengcomm. 2010;12:1410–5.
22. Ross AB, Hall C, Anastasakis K, Westwood A, Jones JM, Crewe RJ. Influence of cation on the pyrolysis and oxidation of alginates. J Anal Appl Pyrol. 2011;91:344–51.
23. Brugnerotto J, Lizardi J, Goycoolea FM, Arguelles-Monal W, Desbrieres J, Rinaudo M. An infrared investigation in relation with chitin and chitosan characterization. Polymer. 2001;42:3569–80.
24. Vijayalakshmi K, Devi BM, Latha S, Gomathi T, Sudha PN, Venkatesan J, et al. Batch adsorption and desorption studies on the removal of lead (II) from aqueous solution using nanochitosan/sodium alginate/microcrystalline cellulose beads. Int J Biol Macromol. 2017;104:1483–94.
25. Abdelmalek BE, Sila A, Haddar A, Bougatef A, Ayadi MA. β-chitin and chitosan from squid gladius: biological activities of chitosan and its application as clarifying agent for apple juice. Int J Biol Macromol. 2017;104: 953–62.
26. Afshar HA, Ghaee A. Preparation of aminated chitosan/alginate scaffold containing halloysite nanotubes with improved cell attachment. Carbohydr Polym. 2016;151:1120–31.
27. Kavaklı C, Barsbay M, Tilki S, Güven O, Kavaklı PA. Activation of polyethylene/polypropylene nonwoven fabric by radiation-induced grafting for the removal of Cr(VI) from aqueous solutions. Water Air Soil Pollut. 2016; 227:473.
28. Bhatt R, Sreedhar B, Padmaja P. Chitosan supramolecularly cross linked with trimesic acid – facile synthesis, characterization and evaluation of adsorption potential for chromium(VI). Int J Biol Macromol. 2017;104: 1254–66.
29. Fan GD, Lin RJ, Su ZY, Lin XY, Xu RX, Chen W. Removal of Cr(VI) from aqueous solutions by titanate nanomaterials synthesized via hydrothermal method. Can J Chem Eng. 2017;95:717–23.
30. Asthana A, Verma R, Singh AK, Susan MA. Glycine functionalized magnetic nanoparticle entrapped calcium alginate beads: a promising adsorbent for removal of cu(II) ions. J Environ Chem Eng. 2016;4:1985–95.
31. Kahu SS, Shekhawat A, Saravanan D, Jugade RM. Two fold modified chitosan for enhanced adsorption of hexavalent chromium from simulated wastewater and industrial effluents. Carbohydr Polym. 2016;146:264–73.
32. Yan YZ, An QD, Xiao ZY, Zheng W, Zhai SG. Flexible core-shell/bead-like alginate@PEI with exceptional adsorption capacity, recycling performance toward batch and column sorption of Cr(VI). Chem Eng J. 2017;313:475–86.
33. Igberase E, Osifo P, Ofomaja A. The adsorption of copper (II) ions by polyaniline graft chitosan beads from aqueous solution: equilibrium, kinetic and desorption studies. J Environ Chem Eng. 2014;2:362–9.
34. Ren HX, Gao ZM, Wu DJ, Jiang JH, Sun YM, Luo CW. Efficient Pb(II) removal using sodium alginate–carboxymethyl cellulose gel beads: preparation, characterization, and adsorption mechanism. Carbohydr Polym. 2016;137: 402–9.
35. Houari B, Louhibi S, Tizaoui K, Boukli-hacene L, Benguella B, Roisnel T, et al. New synthetic material removing heavy metals from aqueous solutions and wastewater. Arab J Chem. In press.
36. Doke KM, Khan EM. Equilibrium, kinetic and diffusion mechanism of Cr(VI) adsorption onto activated carbon derived from wood apple shell. Arab J Chem. 2017;10:S252–60.
37. Ngah WSW, Fatinathan S. Pb(II) biosorption using chitosan and chitosan derivatives beads: equilibrium, ion exchange and mechanism studies. J Environ Sci. 2010;22:338–46.
38. Sharma G, Naushad M, Al-Muhtaseb AH, Kumar A, Khan MR, Kalia S, et al. Fabrication and characterization of chitosan-crosslinked-poly(alginic acid) nanohydrogel for adsorptive removal of Cr(VI) metal ion from aqueous medium. Int J Biol Macromol. 2017;95:484–93.
39. Karthik R, Meenakshi S. Removal of Cr(VI) ions by adsorption onto sodium alginate-polyaniline nanofibers. Int J Biol Macromol. 2015;72:711–7.
40. Gedam AH, Dongre RS, Bansiwal AK. Synthesis and characterization of graphite doped chitosan composite for batch adsorption of lead(II) ions from aqueous solution. Adv Mater Lett. 2015;6:59–7.
41. Soltani RDC, Khorramabadi GS, Khataee AR, Jorfi S. Silica nanopowders/ alginate composite for adsorption of lead (II) ions in aqueous solutions. J Taiwan Inst Chem Eng. 2014;45:973–80.